主办 中国地理学会环境遥感分会
中国科学院遥感与数字地球研究所
出版 科学出版社

JOURNAL OF REMOTE SENSING
遥感学报

2013年 Vol.17 第17卷 No.4 第4期 ISSN 1007-4619 CN11-3841 / TP CODEN YXAUAB

2010年中国土地覆被遥感监测数据集（ChinaCover2010）

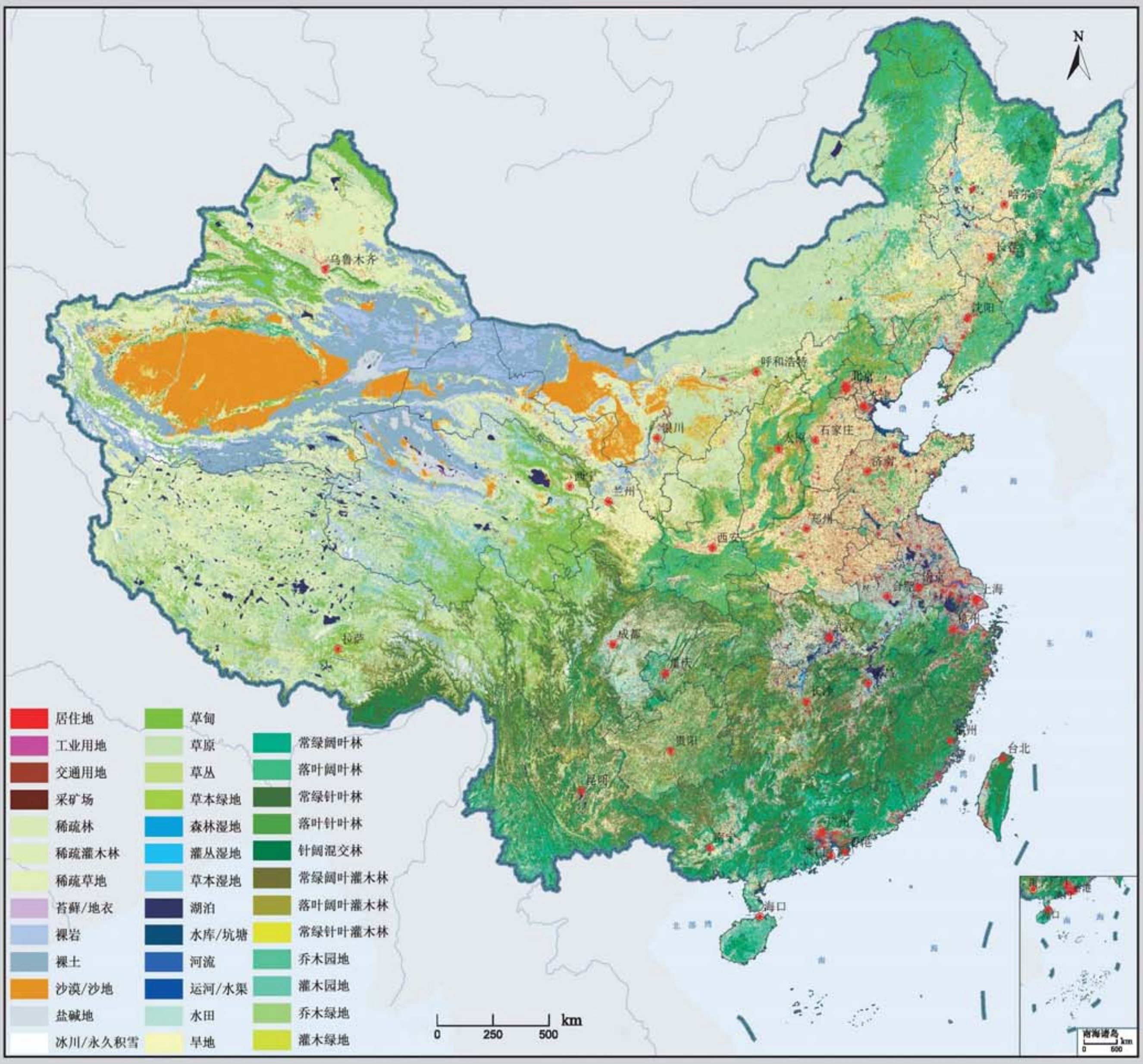

百种中国杰出学术期刊

遥 感 学 报

Yaogan Xuebao

第 17 卷　　第 4 期　　2013 年 7 月

目　　次

JOURNAL OF REMOTE SENSING

(**Vol. 17 No. 4 July, 2013**)

CONTENTS

(to be continued to Inside Back Cover)

(continued from Contents page)

Haze: Remote Sensing

Multi-look SAR image segmentation based on voronoi tessellation technique and EM/MPM algorithm

ZHAO Quanhua[1], **LI Yu**[1], **HE Xiaojun**[2], **SONG Weidong**[1]

1. *School of Geomatics, Liaoning Technical University, Fuxin* 123000, *China*;
2. *College of Innovation and Practice, Liaoning Technical University, Fuxin* 123000, *China*

Abstract: We propose a novel multi-look synthetic aperture radar image segmentation method that combines Voronoi tessellation, expectation maximization (EM), and maximization of the posterior marginal (MPM) technology. The image domain is partitioned into a group of sub-regions by Voronoi tessellation, each of which is a component of homogeneous regions. Then a multi-look SAR image is modeled on the supposition that the intensities of pixels in each homogenous region satisfy an identical and independent gamma distribution. The image segmentation model is constructed based on the Bayesian paradigm. Finally, the EM/MPM algorithm, which integrates the EM algorithm for model parameter estimation and the MPM algorithm for image segmentation, is implemented. The proposed method expands pixel-based MRF to region-based MRF and achieves optimal segmentation and parameter estimation simultaneously. Results obtained from both real RADARSET-I/II and simulated SAR intensity images indicate that the proposed method is efficient and promising.

Key words: Voronoi tessellation, EM/MPM, SAR, image segmentation

CLC number: P223 **Document code**: A

Citation format: **Zhao Q H, Li Y, He X J and Song W D. 2013. Multi-look SAR image segmentation based on voronoi tessellation technique and EM/MPM algorithm. Journal of Remote Sensing, 17(4): 841−854 [DOI: 10.11834/jrs.20132239]**

1 INTRODUCTION

Synthetic Aperture Radar (SAR), an advanced acquisition technology of remote sensing data acquisition, has been applied in numerous fields, such as environmental and disaster monitoring. Image segmentation is the basic and key technology for SAR image processing. To reduce the speckle noise inherent in SAR images, a multi-look SAR image is often obtained via incoherent multi-process technology. The main methods currently used in SAR image processing include region-based, edge-based, and cluster-based technology (Xu, et al., 2010). Regional and statistical-based methods are most valuable because of the statistical characteristics of image speckle noise and pixel value (Dong, et al., 2003). Regional-based method search or model-related region representative technology includes segment-fusion technology (Zhang, et al., 2010; Li, et al., 2003), regional-based Bayesian segmentation technology (Song, et al., 2010; Wong, et al., 2010), and active contour model (Wang, et al., 2010). However, such methods do not consider the correlations among pixels, among regions, and between pixels and regions, so these methods cannot fully use the statistical properties and correlation of different regions of SAR images.

With improvements in SAR image resolution, introducing the correlation hidden in adjacent pixels has become essential in modeling SAR images. Numerous models have been proposed toward this end. Among these models, Markov random field (MRF) models are commonly considered, in which MRF is used to model the joint probability distribution of pixel intensities in terms of local spatial interactions. However, MRF has the following drawbacks in modeling high-resolution remote sensing images. (1) Because MRF model-based image segmentation allows spatial interaction only between neighbor pixels, defining the global correlation among pixels is difficult, whereas a pixel-based MRF model hardly solves the geometry noise problem caused by high resolution in SAR image processing. (2) Small error segmentation areas in statistical homogeneous regions result from the speckle noise inherent in SAR images. To reduce the speckle effect, processing SAR images is necessary via region-based rather than pixel-based methods. Thus, a class of geometry tessellation-based methods is proposed (Green, 1995; Dryden, et al., 2006). The idea behind these methods is that the image domain is first partitioned into sub-regions by a tessellation technique, and then the extent of MRF is explored to model the relationship between sub-regions instead of neighbor pixels. The work of Li and Li (2010) demonstrates the use of a geometry tessellation-based method that integrates Voronoi tessellation, Bayesian inference, and maximum a posterior (MAP) algorithms in SAR image segmentation. Although MAP criterion (Comer,

Received: 2012-08-20; **Accepted**: 2012-11-16; **Version of record first published**: 2012-11-23

Foundation: National Nature Science Foundation of China (No.41271435); The Open Research Fund of Key Laboratory of Digital Earth Science, Center for Earth Observation and Digital Earth, Chinese Academy of Science (No.2012LDE013)

First author biography: ZHAO Quanhua(1978—), female, Ph.D., associate professor. Her main research interests are modeling and analysis of remote sensing images, as well as application of stochastic geometry in remote sensing image processing. She has published over 10 papers. E-mail: zqhlby@163.com

et al., 2011) produces meaningful segmentation in numerous cases, it has several disadvantages besides the computational cost. MAP-based algorithms are incomplete and require prior knowledge of estimated parameters. To solve these problems, Comer and Delp (2000) propose the Expectation Maximization/Maximization of the Posterior Marginal (EM/MPM) algorithm to estimate parameters and segment textured images simultaneously. The EM/MPM algorithm combines the Expectation Maximization (EM) algorithm for parameter estimation with the Maximization of the Posterior Marginal (MPM) algorithm for segmentation. Following the methods proposed by Comer and Delp (2000) and Li and Li (2010), this study presents a novel multi-look SAR image segmentation method that combines Voronoi tessellation, EM/MPM technology.

2 MULTI-LOOK SAR IMAGE MODEL

A multi-look SAR image, $z=\{z_i(x_i,y_i);(x_i,y_i)\in \boldsymbol{D}, i=1,\cdots,n\}$, where i is the index of pixels, z_i is the intensity of pixel (x_i, y_i) is the site of pixel i, $\boldsymbol{D}$ is the domain of the image, and n is the number of pixels of z, can be considered a realization of the discrete random field defined in $\boldsymbol{D}$, $\boldsymbol{Z}=\{\boldsymbol{Z}_i(x_i,y_i);(x_i,y_i)\in\boldsymbol{D}; i=1,\cdots,n\}$, where $\boldsymbol{Z}_i$ denotes the random variable for pixel intensity. We let $\boldsymbol{\Omega}_Z$ be the space of all possible realizations of $\boldsymbol{Z}$.

To model the multi-look SAR image, Voronoi tessellation is used to partition the domain of the image (Li & Li, 2010). With the collection of generating points, $\boldsymbol{G}=\{(u_j,v_j):(u_j,v_j)\in\boldsymbol{D}; j=1,\cdots,m\}$, Voronoi tessellation partitions $\boldsymbol{D}$ into m Voronoi polygons, $\boldsymbol{P}=\{\boldsymbol{P}_j: j=1,\cdots,m\}$, where $\boldsymbol{P}_j$ is the j^{th} polygon induced by the generating point (u_j, v_j) and can be defined as

$$\boldsymbol{P}_j=\{(x,y);d((x,y),(u_j,v_j))\leqslant d((x,y),(u_{j'},v_{j'})),(u_j,v_j),(u_{j'},v_{j'})\in\boldsymbol{G}, j\neq j\} \quad (1)$$

where d is the Euclidian distance of two points in a plan. Fig.1 illustrates a Voronoi tessellation with six generating points.

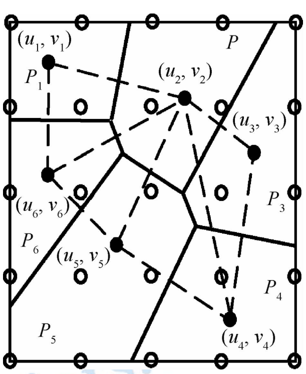

Fig.1 Voronoi tessellation with six generating points

We assume that the generating points are uniformly and independently distributed on $\boldsymbol{D}$. Thus, their joint probability distribution function (PDF) can be expressed as

$$p(\boldsymbol{G}\mid m)=\prod_{j=1}^{m}p(u_j,v_j)=\prod_{j=1}^{m}\frac{1}{\mid\boldsymbol{D}\mid}=\mid\boldsymbol{D}\mid^{-m} \quad (2)$$

where $\mid\boldsymbol{D}\mid$ is the area of image domain $\boldsymbol{D}$. We assume that the number of generating points m follows Poisson distribution with a mean λ, so the PDF can be written as

$$p(m)=\frac{\lambda^m}{m!}\exp(-\lambda) \quad (3)$$

We assign each polygon $\boldsymbol{P}_j$ a random label variable, $\boldsymbol{L}_j\in\{1,\cdots,k\}$, where k is the number of homogeneous regions and is known a prior to indicate the homogeneous region to which the polygon belongs. As a result, the set of all labels $\boldsymbol{L}=\{\boldsymbol{L}_j; j=1,\cdots,m\}$ forms a label field, and its realization responds to a segmentation. To model the label field, an improved Potts model is used:

$$p(\boldsymbol{L}\mid\boldsymbol{G},m)=\frac{1}{A}\exp\Big(-\sum_{\{\boldsymbol{L}_j,\boldsymbol{L}_{j'}\}\in\boldsymbol{NP}}\eta t(\boldsymbol{L}_j,\boldsymbol{L}_{j'})\Big) \quad (4)$$

where $\boldsymbol{NP}$ denotes the set of neighbor polygons (any two Voronoi polygons are neighbors if and only if they have a commute boundary), A is a normalized constant, η is a constant for the interaction of neighbor polygons, and $t(x,y)$ is an indicator expressed as

$$t(x,y)=\begin{cases}0, & \text{if } x=y\\ 1, & \text{if } x\neq y\end{cases} \quad (5)$$

We assume that the intensities in one Voronoi polygon follow an indicial and independent gamma distribution (Lee, et al., 1994; Dong, et al., 2003), that is:

$$p(\boldsymbol{Z}_i\mid(x_i,y_i)\in\boldsymbol{P}_j,\boldsymbol{L}_j=l,\boldsymbol{\beta}_l)=\frac{1}{\Gamma(\alpha)}\frac{\boldsymbol{Z}_i^{\alpha-1}}{\boldsymbol{\beta}_l^{\alpha}}\exp\Big(-\frac{\boldsymbol{Z}_i}{\boldsymbol{\beta}_l}\Big) \quad (6)$$

where $\Gamma(\cdot)$ is the gamma function, and α and $\boldsymbol{\beta}_l$ are the scale and shape parameters, respectively. For a multi-look SAR image, α is equal to the number of its looks (Lee, et al., 1994; Dong, et al., 2003).

Eq.(6) indicates that the joint PDF of the pixels in a Voronoi polygon $\boldsymbol{P}_j$ can be expressed as

$$p(\boldsymbol{Z}_j\mid\boldsymbol{L}_j=l,\boldsymbol{\beta}_l)=\prod_{(x_i,y_i)\in\boldsymbol{P}_j}\frac{1}{\Gamma(\alpha)}\frac{\boldsymbol{Z}_i^{\alpha-1}}{\boldsymbol{\beta}_l^{\alpha}}\exp\Big(-\frac{\boldsymbol{Z}_i}{\boldsymbol{\beta}_l}\Big) \quad (7)$$

where $\boldsymbol{Z}_j=\{\boldsymbol{Z}_i;(x_i,y_i)\in\boldsymbol{P}_j\}$. We assume that the PDFs of all the above Voronoi polygons are independent, so the multi-look SAR image model can be expressed below.

$$p(\boldsymbol{Z}\mid\boldsymbol{L},\boldsymbol{G},\boldsymbol{\beta},m)=\prod_{j=1}^{m}p(\boldsymbol{Z}_j\mid\boldsymbol{L}_j)=\prod_{j=1}^{m}\prod_{(x_i,y_i)\in\boldsymbol{P}_j}\frac{1}{\Gamma(\alpha)}\frac{\boldsymbol{Z}_i^{\alpha-1}}{\boldsymbol{\beta}_l^{\alpha}}\exp\Big(-\frac{\boldsymbol{Z}_i}{\boldsymbol{\beta}_l}\Big) \quad (8)$$

where $\boldsymbol{\beta}=(\boldsymbol{\beta}_1,\cdots,\boldsymbol{\beta}_k)$.

To segment a multi-look SAR image $\boldsymbol{Z}$, deriving the joint PDF of $\boldsymbol{L}$ and $\boldsymbol{G}$ given $\boldsymbol{Z}$ is necessary. Using Bayes' rule, as well as Eq.(4) and Eq.(8), we have

$$\begin{aligned}p(\boldsymbol{L},\boldsymbol{G},m\mid\boldsymbol{Z},\boldsymbol{\beta})&=\frac{p(\boldsymbol{Z}\mid\boldsymbol{L},\boldsymbol{\beta})p(\boldsymbol{L}\mid\boldsymbol{G},m)p(\boldsymbol{G}\mid m)p(m)}{p(\boldsymbol{Z}\mid\boldsymbol{\beta})}=\\ &\frac{1}{p(\boldsymbol{Z}\mid\boldsymbol{\beta})}\times\mid\boldsymbol{D}\mid^{-m}\times\frac{\lambda^m}{m!}\exp(-\lambda)\times\\ &\prod_{j=1}^{m}\prod_{(x_i,y_i)\in\boldsymbol{P}_j}\frac{1}{\Gamma(\alpha)}\frac{Z_i^{\alpha-1}}{\boldsymbol{\beta}_l^{\alpha}}\exp\Big(-\frac{\boldsymbol{Z}_i}{\boldsymbol{\beta}_l}\Big)\times\\ &\frac{1}{A}\exp\Big[-\sum_{\{L_j,L_{j'}\}\in\boldsymbol{NP}}\eta t(\boldsymbol{L}_j,\boldsymbol{L}_{j'})\Big]\end{aligned} \quad (9)$$

Because A and $p(\boldsymbol{Z}\mid\boldsymbol{\beta})$ do not depend on $\boldsymbol{L}$ and $\boldsymbol{G}$, they are not considered in the optimization to segment the SAR image.

3 EM/MPM ALGORITHM

The EM/MPM algorithm is proposed for image segmentation after modeling the multi-look SAR image. The proposed algorithm includes two steps: the MPM phase for segmentation and the EM phase for estimating parameter $\boldsymbol{\beta}$.

3.1 MPM multi-look SAR segmentation

In the MPM phase, we assume that $\boldsymbol{\beta}$ is known, and we consider the segmentation as an optimization problem. The optimization criterion is the minimization of the expected value of the number of misclassified pixels (Comer & Depth, 2000). Minimizing this expected value is equivalent to maximizing $p(\boldsymbol{L}_j=l, \boldsymbol{G} \mid \boldsymbol{Z}=z)$ over all $l \in \{1, \cdots, k\}$ for Voronoi polygon $\boldsymbol{P}_j (j = 1, \cdots, m)$ (Marroquin, et al., 1987). Thus, to find the MPM estimate of the label field $\boldsymbol{L}$, determining the l for each $\boldsymbol{P}_j$ is necessary. $\boldsymbol{P}_j$ maximizes

$$p(\boldsymbol{L}_j = l \mid \boldsymbol{Z} = z) = p(l, \boldsymbol{G} \mid \boldsymbol{Z}, \boldsymbol{\beta}) = \sum_{l \in \Omega_{l,j}, \boldsymbol{G} \in \boldsymbol{\Omega}_G} p(l, \boldsymbol{G} \mid \boldsymbol{Z}, \boldsymbol{\beta}) \tag{10}$$

where $\Omega_{l,j} = \{\boldsymbol{l}; l_j = l\}$; Ω_G denotes the space of the point collection, and l is the realization of the label field $\boldsymbol{L}$. In fact, calculating accurately the marginal probability functions as in Eq.(10) is infeasible. To obtain the MPM estimate of an MRF, Marroquin, et al. (1987) presented an algorithm to approximate marginal probability. In this study, the algorithm is also used to approximate the marginal probabilities of function Eq.(10). The approximation includes (Comer, et al., 2011) designing the random sampler and generating a discrete-time Markov chain $\boldsymbol{L}(t) = \{\boldsymbol{L}_j(t); j=1, \cdots, m\}$, which is based on the PDF in Eq.(9); $\boldsymbol{L}(t)$ is the limiting distribution of the label field $\boldsymbol{L}$. For any initial realization $l(0)$ with a given label field.

$$\lim_{t \to \infty} p(\boldsymbol{L}(t) = l, \boldsymbol{G} \mid \boldsymbol{Z} = z, \boldsymbol{L}(0) = l(0)) = p(l, \boldsymbol{G} \mid z, \boldsymbol{\beta}) \tag{11}$$

As a component $\boldsymbol{L}_j$ of the label field, $\boldsymbol{L}$ can be changed each time during iterative sampling, so the following function is defined as

$$a_{l,j} \equiv \begin{cases} 1, & \text{if} \quad \boldsymbol{L}_j(t) = l \\ 0, & \text{if} \quad \boldsymbol{L}_j(t) \neq l \end{cases} \tag{12}$$

Thus,

$$p(\boldsymbol{L}_j = l, \boldsymbol{G} \mid z, \boldsymbol{\beta}) \approx \frac{1}{T_j} \sum_{t=1}^{T_j} a_{l,j}(t), \quad \forall l, j \tag{13}$$

where T_j is the number of visits to $\boldsymbol{L}_j$ made by the random sampler. Eq.(13) shows how to obtain the MPM estimate of the label field $\boldsymbol{L}$.

In this study, the Metropolis-Hastings (M-H) algorithm is designed for sampling ($\boldsymbol{L}$, $\boldsymbol{G}$). All of the following move operations are implemented during the iterative sample.

(1) Changing the label field. In the label field $\boldsymbol{L} = \{\boldsymbol{L}_j;\ j = 1, \cdots, m\}$, each label $\boldsymbol{L}_j$, $j = 1, \cdots, m$, is extracted with equal probability $(1/m)$, and $\boldsymbol{L}_j$ is changed. Proposed label $\boldsymbol{L}_j{}^*$ is extracted with equal probability $(1/k)$, and it satisfies the condition. Acceptance probability can be calculated as

$$a_L(\boldsymbol{L}_j, \boldsymbol{L}_j{}^*) = \min\left\{1, \frac{\prod_{(x_i,y_i) \in \boldsymbol{P}_j} \frac{1}{(\boldsymbol{\beta}_{\boldsymbol{L}_j *})^{\alpha}} \exp\left[-\frac{\boldsymbol{Z}_i}{\boldsymbol{\beta}_{\boldsymbol{L}_j *}}\right] \exp\left[-\sum_{\boldsymbol{P}_{j'} \in \boldsymbol{NP}_j} \eta t(\boldsymbol{L}_j{}^*, \boldsymbol{L}_{j'})\right]}{\prod_{(x_i,y_i) \in \boldsymbol{P}_j} \frac{1}{(\boldsymbol{\beta}_{\boldsymbol{L}_j})^{\alpha}} \exp\left[-\frac{\boldsymbol{Z}_i}{\boldsymbol{\beta}_{\boldsymbol{L}_j}}\right] \exp\left[-\sum_{\boldsymbol{P}_{j'} \in \boldsymbol{NP}_j} \eta t(\boldsymbol{L}_j, \boldsymbol{L}_{j'})\right]}\right\} \tag{14}$$

where $\boldsymbol{NP}_j$ is the set of the neighbor Voronoi polygons of $\boldsymbol{P}_j$.

(2) Moving the generating points. First, a generating point (u_j, v_j) is extracted from the set of generating points $\boldsymbol{G} = \{(u_j, v_j) \in \boldsymbol{D};\ j = 1, \cdots, m\}$ with equal probability $(1/m)$. The proposed generating point $(u_j{}^*, v_j{}^*)$ is randomly distributed in the area of polygon $\boldsymbol{P}_j$. The acceptance probability of $(u_j{}^*, v_j{}^*)$ can be written as

$$a_{(u,v)}((u_j, v_j), (u_j{}^*, v_j{}^*)) = \min\left\{1, \frac{\prod_{P_{j'} \in \{\boldsymbol{P}_j *, \boldsymbol{PN}_j *\}} \prod_{(x_i,y_i) \in \boldsymbol{P}_{j'}} \frac{1}{(\boldsymbol{\beta}_{\boldsymbol{L}_{j'}})^{\alpha}} \exp\left[-\frac{\boldsymbol{Z}_i}{\boldsymbol{\beta}_{\boldsymbol{L}_{j'}}}\right]}{\prod_{\boldsymbol{P}_{j'} \in \{\boldsymbol{P}_j, \boldsymbol{PN}_j\}} \prod_{(x_i,y_i) \in \boldsymbol{P}_{j'}} \frac{1}{(\boldsymbol{\beta}_{\boldsymbol{L}_{j'}})^{\alpha}} \exp\left[-\frac{\boldsymbol{Z}_i}{\boldsymbol{\beta}_{\boldsymbol{L}_{j'}}}\right]}\right\} \tag{15}$$

(3) Adding or deleting generating points. We assume that the set of generating points is $\boldsymbol{G} = \{(u_1, v_1), \cdots, (u_j, v_j), \cdots (u_m, v_m)\}$. To add generating points, a Voronoi polygon $\boldsymbol{P}_j$ is chosen, and a proposed generating point is extracted in this polygon with label $\boldsymbol{L}_{m+1}$, namely, $(u_{m+1}{}^*, v_{m+1}{}^*)$. Correspondingly, the set of generating points is $\boldsymbol{G}^* = \{(u_1, v_1), \cdots, (u_j, v_j), \cdots (u_m, v_m), (u_{m+1}{}^*, v_{m+1}{}^*)\}$. Eq.(1) states that a new Voronoi tessellation is formed, $\boldsymbol{P}^* = \{\boldsymbol{P}_1{}^*, \cdots, \boldsymbol{P}_m{}^*, \boldsymbol{P}_{m+1}{}^*\}$. Because $(u_{m+1}{}^*, v_{m+1}{}^*)$ is located in $\boldsymbol{P}_j$, the newly generated polygon $\boldsymbol{P}_{m+1}{}^*$ only changes the polygon $\boldsymbol{P}_j$ and its neighborhood polygons. The label $\boldsymbol{L}_{m+1}{}^*$ of the polygon $\boldsymbol{P}_{m+1}{}^*$ is extracted with equal probability $(1/k)$ in the $\{1, \cdots, k\}$. Thus, the proposed label field is $\boldsymbol{L}^* = \{\boldsymbol{L}_1{}^*, \cdots, \boldsymbol{L}_j{}^*, \cdots, \boldsymbol{L}_m{}^*, \boldsymbol{L}_{m+1}{}^*\}$, whereas the label $\{\boldsymbol{P}_1{}^*, \cdots, \boldsymbol{P}_m{}^*\}$ remains unchanged. The operation of adding the generating points is accepted by the following probability:

$$a_{G+}(\boldsymbol{G}, \boldsymbol{G}^*) = \min\{1, R\} \tag{16}$$

where

$$R = \frac{\prod_{j=1}^{m+1} \prod_{(x_i,y_i) \in \boldsymbol{P}_j *} \frac{1}{(\boldsymbol{\beta}_{\boldsymbol{L}_j *})^{\alpha}} \exp[-\boldsymbol{Z}_i/\boldsymbol{\beta}_{\boldsymbol{L}_j *}]}{\prod_{j=1}^{m} \prod_{(x_i,y_i) \in \boldsymbol{P}_j} \frac{1}{(\boldsymbol{\beta}_{\boldsymbol{L}_j})^{\alpha}} \exp[-\boldsymbol{Z}_i/\boldsymbol{\beta}_{\boldsymbol{L}_j}]} \times \frac{\prod_{j=1}^{m+1} \exp\left(\sum_{\boldsymbol{P}_{j'} * \in \boldsymbol{PN}_j *} \eta t(\boldsymbol{L}_j{}^*, \boldsymbol{L}_{j'}{}^*)\right) \Big/ \sum_{l=1}^{k} \exp\left(\sum_{\boldsymbol{P}_{j'} * \in \boldsymbol{PN}_j *} \eta t(l, \boldsymbol{L}_{j'}{}^*)\right)}{\prod_{j=1}^{m} \exp\left(\sum_{\boldsymbol{P}_{j'} * \in \boldsymbol{PN}_j *} \eta t(\boldsymbol{L}_j, \boldsymbol{L}_{j'})\right) \Big/ \sum_{l=1}^{k} \exp\left(\sum_{\boldsymbol{P}_{j'} \in \boldsymbol{PN}_j} \eta t(l, \boldsymbol{L}_{j'})\right)} \tag{17}$$

The operation of deleting the generating points is a dual operation of adding generating points, so its acceptable probability can be expressed as

$$a_{G-}(\boldsymbol{G}, \boldsymbol{G}^*) = \min\{1, 1/R\} \tag{18}$$

3.2 EM algorithm for parameter estimation

To implement the M-H sample, parameter $\boldsymbol{\beta}$ needs to be estimated. In this study, the EM algorithm is used to estimate the value of $\boldsymbol{\beta}$ (Masuda, et al., 2011; Xia, et al., 2011; Xu, et al., 2011). An iterative procedure is conducted in the EM algorithm to approximate the maximum-likelihood estimates. Two steps are performed in each iteration: expectation and maximization. We let $\boldsymbol{\beta}(\tau)$ be the estimate of parameter $\boldsymbol{\beta}$ at iteration τ, so the estimate value of $\boldsymbol{\beta}$ at the iteration can be expressed as

$$Q(\boldsymbol{\beta},\boldsymbol{\beta}(\tau-1)) = E[\log p(\boldsymbol{Z}\mid \boldsymbol{L},\boldsymbol{\beta})\mid \boldsymbol{Z}=z,\boldsymbol{\beta}(\tau-1)] + E[\log p(\boldsymbol{L}\mid \boldsymbol{\beta})\mid \boldsymbol{Z}=z,\boldsymbol{\beta}(\tau-1)] \quad (19)$$

Because the PDF of the label field $\boldsymbol{L}$ does not depend on $\boldsymbol{\beta}$, the second term of Eq.(19) is ignored. $\boldsymbol{\beta}(\tau)$ is obtained as the value that maximizes $Q(\boldsymbol{\beta},\boldsymbol{\beta}(\tau-1))$, and $\boldsymbol{\beta}(\tau)$ satisfies

$$Q(\boldsymbol{\beta}(\tau),\boldsymbol{\beta}(\tau-1)) \geqslant Q(\boldsymbol{\beta},\boldsymbol{\beta}(\tau-1)) \quad \forall \boldsymbol{\beta}\in \boldsymbol{\Omega}_{\beta} \quad (20)$$

where $\boldsymbol{\Omega}_{\beta}$ is the space of all possible values of $\boldsymbol{\beta}$. After substituting Eq.(8) into Eq.(19), differentiating, and setting to zero, the result of $\boldsymbol{\beta}(\tau) = (\boldsymbol{\beta}_1(\tau),\cdots,\boldsymbol{\beta}_k(\tau))$ is as.

$$\boldsymbol{\beta}_l(\tau) = \frac{1}{\alpha N_l(\tau)}\sum_{P_j\in \boldsymbol{P}_l} p(\boldsymbol{L}_j = l\mid \boldsymbol{Z},\boldsymbol{\beta}(\tau-1))\sum_{(x_i,y_i)\in \boldsymbol{P}_j}\boldsymbol{Z}_i \quad (21)$$

where $\boldsymbol{P}_l = \{\boldsymbol{P}_j;\ \boldsymbol{L}_j = l\}$, $N_l(\tau) = \sum_{P_j\in \boldsymbol{P}_l} N_j p(\boldsymbol{L}_j = l\mid \boldsymbol{Z},\boldsymbol{\beta}(\tau-1))$, $N_j = \#\boldsymbol{Z}_j$. The exact computation of $p(\boldsymbol{L}_j = l\mid \boldsymbol{Z},\boldsymbol{\beta})$ is infeasible. Thus, Eq.(13) is used in this study to obtain the estimate of $p(\boldsymbol{L}_j = l\mid \boldsymbol{Z},\boldsymbol{\beta})$ and to compute Eq.(21) to obtain the estimate of parameter $\boldsymbol{\beta}$.

3.3 EM/MPM algorithm for segmentation

The EM/MPM algorithm uses the EM algorithm and MPM algorithm, which combine the MPM algorithm for segmentation and the EM algorithm for parameter estimation. The procedures of the EM/MPM algorithm are described as below

(1) Parameter $\boldsymbol{\beta}$, noted as $\boldsymbol{\beta}(0)$, is initialized.

(2) Parameter $\boldsymbol{\beta}(\tau-1)$ is used to implement the MPM algorithm for T_p times (T_p = 500 in this study) to obtain the MPM estimate of the label field $\boldsymbol{L}$ by Eq.(13).

(3) Step (2) is used to obtain the MPM estimate of the label field $\boldsymbol{L}$, and this estimate is substituted into Eq.(21) to obtain $\boldsymbol{\beta}(\tau)$ of the $\boldsymbol{\beta}$ estimate.

(4) The step involving Eq.(2) is repeated until the expected total number of iterations is reached.

4 EXPERIMENTAL RESULTS AND DISCUSSION

To validate the feasibility and effectiveness of the proposed algorithm, synthetic and real SAR intensity images are used. First, a synthetic SAR intensity image with four looks, five homogeneous regions, and 128 × 128 pixels resolution is created. Fig.2(a) presents the template of homogeneous regions, in which the numbers 1—5 indicate the different homogeneous regions. Table 1 lists the parameters of gamma distribution for the corresponding homogenous regions. Fig. 2(b) shows the created synthetic SAR intensity image.

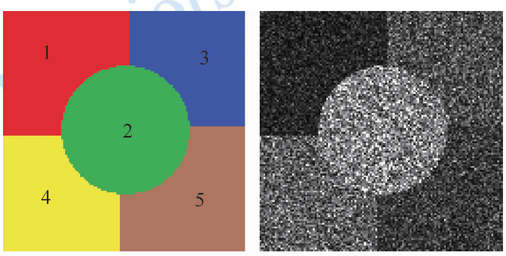

(a) Template (b) Synthetic SAR image

Fig.2 Synthetic image

Table 1 Gamma distribution parameters for the different homogeneous regions

Parameters	Homogeneous regions				
	1	2	3	4	5
α	4	4	4	4	4
β	10	35	20	25	15

Fig.3(a) and Fig.3(b) illustrate the final Voronoi tessellation and optimal segmentation results after 500 iterations for MPM and 100 iterations for EM estimation. The method presented in this study is essentially an extension of the pixel-based MRF proposed by Cao, et al. (2005) and Comer and Delp (2000). For comparison, Fig.3(c) shows the segmentation results of the pixel-based MRF algorithm. Comparing the two segmentation results shown in Fig. 3(b) and Fig. 3(c) indicates that the method presented in this study can segment the five homogeneous regions well, whereas the pixel-based MRF almost fails to distinguish the regions.

(a) Final Voronoi tessellation (b) Optimal segmentation (c) Segmentation from the pixel-based MRF algorithm

Fig.3 Segmentation results

Table 2 lists the estimated values of the gamma distribution parameters and their percentage errors. The figures indicate that the proposed algorithm can accurately estimate the model parameters.

Table 2 Estimated scale parameters of the homogeneous regions and their errors

Parameters		Homogeneous regions				
		1	2	3	4	5
Proposed method	$\boldsymbol{\beta}_e$	10.05	33.64	20.04	24.62	15.12
	e_{β}/%	0.47	1.37	0.04	0.38	0.12
MRF	$\boldsymbol{\beta}_e$	11.27	35.37	16.18	24.38	12.50
	e_{β}/%	1.27	0.37	3.72	0.62	2.50

To visually illustrate the accuracy of the segmented results, the outlines of the segmented homogeneous regions are delineated and overlaid on the synthetic SAR image. Fig.4 shows that the delineated outlines match well the boundaries of the homogeneous regions.

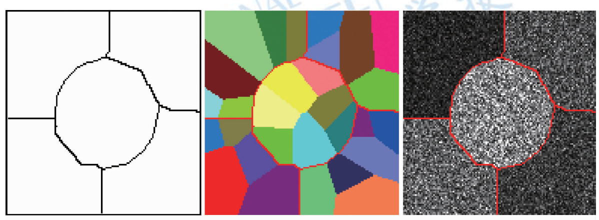

(a) Extracted outline (b) Overlay of the extracted outline on Voronoi tessellation (c) Overlay of the extracted outline on a synthetic image

Fig.4 Segmentation results

Fig.5 reports the changes in the scale parameters during 500 iterations and indicates that the stable values of the estimated parameters finally converge.

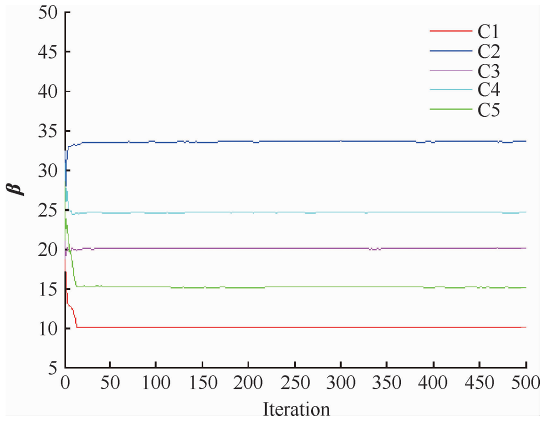

Fig.5　Changes in scale parameters during 500 iterations

Statistical measures, including the producer's accuracy, user's accuracy, overall accuracy, and kappa coefficient, are used to measure segmentation accuracy. Table 3 provides the results of the proposed method and the pixel-based MRF method. Table 3 indicates that the Kappa coefficient for the segmented result is up to 0.99. General interpretation rules to assess thematic accuracy indicate that a Kappa coefficient from 0.81 to 1.00 is almost perfect (Congalton & Green, 2008).

Table 3　User's accuracy, producer's accuracy, overall accuracy, and Kappa coefficient

Method	Measure/%	Homogeneous regions				
		1	2	3	4	5
Proposed method	User's accuracy	99.61	99.06	99.63	99.12	99.22
	Producer's accuracy	99.94	99.20	99.42	99.84	98.41
	Overall accuracy			99.34		
	Kappa			0.99		
Pixel-based MRF method	User's accuracy	51.01	75.93	65.37	51.48	36.86
	Producer's accuracy	26.42	79.98	65.35	56.15	40.26
	Overall accuracy			44.59		
	Kappa			0.31		

In this study, the number of polygons in Voronoi tessellation m is set as a random variable. To test the effect of initial m_0 on the final segmentation, the segmentation results from m_0 = 48, 64, 80, 96, and 112 are compared. Fig.6 presents the changes in m during 500 iterations with different m_0. The final numbers of m after 500 iterations are 29, 30, 36, 35, and 33. In other words, the proposed method attempts to fit all the homogeneous regions with the polygons as less as possible.

Real SAR intensity images are also used for validation. Fig.7 shows three RADARSAT-Ⅰ/Ⅱ SAR intensity images with number of looks 2, 3, 4 and with homogeneous regions 4, 3, 4.

Fig.8(a) to Fig.8(c) provide the optimal segmentations, Fig.8(d) to Fig.8(f) show the extracted boundaries of the segmented homogeneous regions, and Fig.8(g) to Fig.8(i) and Fig.8(j) to Fig.8(l) illustrate the overlaying of the extracted boundaries on Voronoi tessellations and testing images. All of these images show that the proposed method can segment real SAR intensity images well.

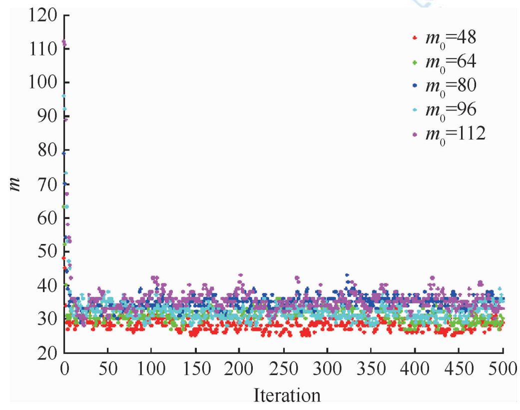

Fig.6　Change in m during 500 iterations

(a) First　(b) Second　(c) Third

Fig.7　Real SAR intensity images for testing

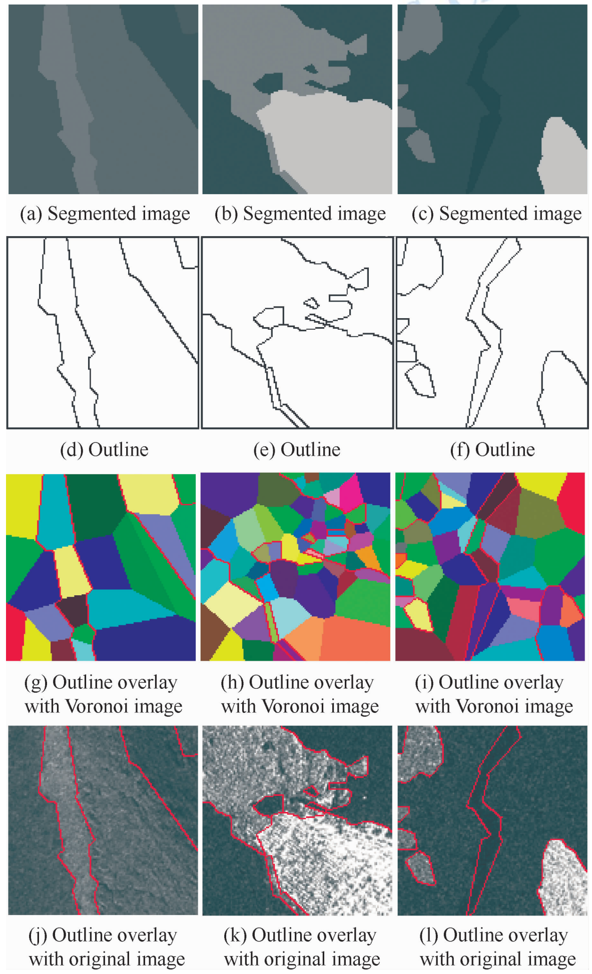

(a) Segmented image　(b) Segmented image　(c) Segmented image

(d) Outline　(e) Outline　(f) Outline

(g) Outline overlay with Voronoi image　(h) Outline overlay with Voronoi image　(i) Outline overlay with Voronoi image

(j) Outline overlay with original image　(k) Outline overlay with original image　(l) Outline overlay with original image

Fig.8　Visual assessment

5 CONCLUSION

This study presents a new segmentation method based on Voronoi tessellation technique and the EM/MPM algorithm. The proposed method is evaluated with real RADATSAT-Ⅱ and synthetic SAR images. The experimental results indicate the efficiency of the proposed segmentation method.

Future research will focus on issues such as developing an algorithm to increase fitting accuracy on the boundaries of segmented regions, comparing the effects of different tessellation schemes (e.g., regular, Poisson, and leave tessellation on segmentation results), and considering the scale and shape parameters of gamma distribution as random variables to improve the accuracy of estimate parameters.

REFERENCES

Cao Y, Sun H and Xu X. 2005. An unsupervised segmentation method based on MPM for SAR images. IEEE Geoscience and Remote Sensing Letters, 2(1): 55−58 [DOI: 10.1109/LGRS.2004.839649]

Comer M L and Delp E J. 2000. The EM/MPM algorithm for segmentation of textured images: analysis and future experimental results. IEEE Transactions on Image Processing, 9(10): 1731−1744 [DOI: 10.1109/83.869185]

Comer M L, Bouman C A, De Graef M and Dimmons J P. 2011. Bayesian methods for image segmentation. JOM Journal of the Minerals, Metals and Materials Society, 63(7): 55−57 [DOI: 10.1007/s11837−011−0113−3]

Congaltonr G and Green K. 2008. Assessing the Accuracy of Remotely Sensed Data: Principles and Practices. Boca Raton: CRC Press, 169−190

Dong Y, Forster B C and Milne A K. 2003. Comparison of radar image segmentation by Gaussian-and Gamma-Markov random field models. International Journal of Remote Sensing, 24(4): 711−722 [DOI: 10.1080/0143116021000013322]

Dryden I L, Farnoosh R and Taylor C C. 2006. Image segmentation using Voronoi polygons and MCMC, with application to muscle fibre images. Journal of Applied Statistics, 33(6): 609−622 [DOI: 10.1080/02664760600679825]

Green P. 1995. Reversible jump MCMC computation and Bayesian model determination. Biometrika, 82(4): 711−732 [DOI: 10.1093/biomet/82.4.711]

Lee J S, Hoppel K W, Mango S A and Miller A R. 1994. Intensity and phase statistics of multilook polarimetric and interferometric SAR imagery. IEEE Transactions on Geoscience and Remote Sensing, 32(5): 1017−1028 [DOI: 10.1109/36.312890]

Li S D, Zhang C and Wang Z Z. 2003. SAR image segmentation by likelihood criterion. Journal of Remote Sensing, 7(2): 118−124

Li Y and Li J. 2010. Segmentation of SAR intensity imagery with a Voronoi tessellation, Bayesian inference, and reversible jump MCMC algorithm. IEEE Transactions on Geoscience and Remote Sensing, 48(4): 1872−1881 [DOI: 10.1109/TGRS.2009.2033588]

Marroquin J, Mitter S and Pojjio T. 1987. Probabilistic solution of ill-posed problems in computational vision. Journal of the American Statistical Association, 82(397): 76−89

Masuda Y, Tateyama T, Wei X, Zhou J Y, Wakamiya M, Kanasaki S, Furukawa A and Chen Y W. 2011. Liver tumor detection in CT images by adaptive contrast enhancement and the EM/MPM algorithm // Proceedings of the 18th IEEE International Conference on Image Processing. Brussels, Belgium: IEEE: 1421−1424 [DOI: 10.1109/ICIP.2011.6115708]

Song X F, Wang S and Liu F. 2010. SAR image segmentation using Markov random field based on regions and Bayes belief propagation. Acta Electronica Sinica, 38(12): 2810−2815

Wang X L and Li C S. 2010. SAR image segmentation using level set evolution without prior information. Journal of Beijing University of Aeronautics and Astronautics, 36(7): 841−844

Wong A, Yu P, Zhang W and Clausi D A. 2010. IceSynth II: synthesis of SAR sea-ice imagery using region based posterior sampling. IEEE Geoscience and Remote Sensing Letters, 7(2): 348−351 [DOI: 10.1109/LGRS.2009.2035136]

Xia H Y and Guo P. 2011. A shadow detection of Remote Sensing images based on statistical texture features. Journal of Remote Sensing, 15(4): 785−791

Xu X Z, Ding S F, Shi Z Z and Jia W K. 2010. New theories and methods of image segmentation. Acta Electronica Sinica, 38(S1): 76−82

Xu Z H, Huang J G and Zhang Q F. 2011. New method for distributed and quantitative estimation fusion of multi-sensor based on EM algorithm. Journal of Electronics and Information Technology, 33(4): 977−981

Zhang L and Zhu Z D. 2010. Target segmentation for SAR images based on global Maxflow neighbor region grow algorithm. Journal of Nanjing University of Aeronautics and Astronautics, 42(6): 764−768

基于 Voronoi 几何划分和 EM/MPM 算法的多视 SAR 图像分割

赵泉华[1]，李玉[1]，何晓军[2]，宋伟东[1]

1.辽宁工程技术大学 测绘与地理科学学院,辽宁 阜新 123000;
2.辽宁工程技术大学 创新实践学院,辽宁 阜新 123000

摘　要:基于区域和统计的 SAR 分割方法,提出一种结合 Voronoi 划分技术、最大期望值 EM (Expectation Maximization)和最大边缘概率 MPM (Maximization of the Posterior Marginal)算法的多视 SAR 图像分割方法。首先利用 Voronoi 划分将图像域划分成不同的子区域,而每个子区域可以被看成待分割同质区域的一个组成部分,并假设每个子区域内的像素满足同一独立的 Gamma 分布,从而建立多视 SAR 图像模型,并在贝叶斯理论架构下建立图像分割模型,然后结合 EM/MPM 算法进行图像分割和模型参数估计。该方法将基于像元的马尔可夫随机场(Markov Random Field, MRF)模型扩展到基于区域的 MRF 模型,并且能同时有效地获取模型参数估计和基于区域的 SAR 图像最优分割。采用本文算法,分别对 RADARSAT-Ⅰ/Ⅱ SAR 强度图像和合成 SAR 强度图像进行了分割实验,定性和定量的测试结果验证了本文方法的有效性、可靠性和准确性。

关键词:Voronoi 几何划分,EM/MPM 算法,SAR,图像分割

中图分类号:P223　　**文献标志码**:A

引用格式:赵泉华,李玉,何晓军,宋伟东. 2013. 基于 Voronoi 几何划分和 EM/MPM 算法的多视 SAR 图像分割. 遥感学报, 17(4): 841-854

Zhao Q H, Li Y, He X J and Song W D. 2013. Multi-look SAR image segmentation based on voronoi tessellation technique and EM/MPM algorithm. Journal of Remote Sensing, 17(4): 841-854 [DOI: 10.11834/jrs.20132239]

1 引　言

合成孔径雷达 SAR 是一种先进的遥感信息获取手段,已经在农作物、植被提取和海冰、灾害监测等许多领域得到了广泛应用。图像分割是 SAR 图像处理中最为基本和关键的技术。为了消除 SAR 图像所固有的斑点噪声,在 SAR 图像获取过程中往往进行非相干多视处理,从而获得多视 SAR 图像。目前提出了众多的多视 SAR 图像分割算法,主要包括:基于区域的、边界的和聚类的分割方法等(许新征 等,2010)。由于 SAR 图像中固有的斑点噪声及地物目标内像素强度具有统计分布特性,因此,基于区域和统计的方法被认为是最为有效的分割方法(Dong 等, 2003)。基于区域的 SAR 图像分割方法直接搜索或建模图像上的相关区域,典型的技术手段包括:分割-融合技术(张林和朱兆达,2010; 郦苏丹 等,2003)、基于区域的贝叶斯分割(宋晓峰 等,2010;Wong 等, 2010)、主动轮廓模型(王晓亮和李春升,2010)。但以上基于区域的模型没有同时顾及邻域像素间、区域内像素间及区域与区域之间相互关系,即没有充分利用 SAR 图像统计分布特性以及邻近区域的相关性。

随着空间分辨率的增加,在 SAR 图像分割中引入像素强度的空间相关性可以显著提高算法的准确性和可靠性,其中最具代表性的统计模型就是 MRF 模型。但传统 MRF 模型在高分辨率 SAR 图像分割中存在以下问题:(1)MRF 模型的定义是基于邻域像素间的相关性,难以定义全局约束,而且基于像素的处理方法很难解决由高分辨率引起的 SAR 图像中的几何噪声;(2)由于 SAR 图像所特有的

收稿日期:2012-08-20;**修订日期**:2012-11-16;**优先数字出版日期**:2012-11-23

基金项目:国家自然科学基金项目(编号:41271435);中国科学院数字地球重点实验室开放基金项目(编号:2012LDE013)

第一作者简介:赵泉华(1978—　),女,博士,副教授,主要研究方向为遥感图像建模与分析,随机几何在遥感图像处理中的应用。发表学术论文 10 余篇。E-mail: zqhlby@163.com

斑点噪声,误分割像素在统计同质区域内呈现微小的误分区域,从而降低了图像分割精度。为了在图像建模过程中真正引入基于区域的思想,需要预先对图像域进行几何划分,然后建立基于区域的 MRF 模型,其中最常用的是 Voronoi 划分(Green,1995;Dryden 等, 2006),但在以上文献中基于 Voronoi 划分的 MRF 模型仅用于一般图像的分割,并未应用到 SAR 图像分割中。为了充分考虑 SAR 图像的统计分布特性,Li 和 Li(2010)提出了基于几何划分的 SAR 图像统计分割方法,该方法采用最大后验概率 MAP(Maximum A Posterior)算法来获取模型参数估计和图像最优分割。

统计图像分割算法涉及的主要问题包括:图像的统计模型、模型参数估计以及获取最佳分割的优化准则。MAP 算法通常用于获取模型参数估计和图像最优分割(Comer 等, 2011)。但在大多数情况下,MAP 算法在计算上是难以实现的,并且 MAP 算法需要给出模型参数的先验分布规律。为了解决上述 MAP 算法存在的问题,Comer 和 Delp (2000)提出了 EM/MPM (Expectation Maximization/Maximization of the Posterior Marginal)算法,建立了基于像素的 MRF 模型,并且采用 EM/MPM 实现了参数的估计和纹理图像的分割。EM/MPM 算法的目的在于最小化误分像素数的期望值,等价于最大化类别标号的边缘概率。EM/MPM 算法同时利用 EM 实现模型参数估计以及利用 MPM 算法得到最优分割。

为了实现在模型参数先验分布知识未知情况下进行基于区域的统计 SAR 图像最优分割,同时获取更精确的模型参数估计结果,本文将基于 Voronoi 的划分技术和 EM/MPM 算法结合起来进行 SAR 图像分割。首先利用 Voronoi 划分建立基于区域的图像分割模型。在该模型中,图像域被划分成不同的子区域,而每个子区域可以被看成待分割同质区域的一个组成部分,并假设每个子区域内的像素满足同一独立的 Gamma 分布,利用上述多视 SAR 图像模型,在贝叶斯理论 (Comer 等, 2011)架构下建模图像分割问题,然后结合 EM/MPM 算法进行参数估计和图像分割,该方法将基于像素的 MRF 模型扩展到基于区域的 MRF,并且能同时有效地获取模型参数估计和基于区域的 SAR 图像最优分割。

2 多视 SAR 图像模型

多视 SAR 图像 $z=\{z_i(x_i,y_i);(x_i,y_i)\in \boldsymbol{D},i=1,\cdots,n\}$ (其中,i 为像素索引,z_i 为像素 i 的强度,(x_i, y_i)为第 i 个像素点的位置,$\boldsymbol{D}$ 为图像域,n 为总像素数)可以看成定义在 $\boldsymbol{D}$ 上离散随机场 $\boldsymbol{Z}=\{Z_i(x_i,y_i);(x_i,y_i)\in \boldsymbol{D};i=1,\cdots,n\}$(其中,$Z_i$ 为表征第 i 个像素强度的随机变量)的一个实现。设 $\boldsymbol{Z}$ 所有可能的实现构成的空间记为 $\boldsymbol{\Omega}_{\boldsymbol{Z}}$。

为了建模多视 SAR 图像,首先利用 Voronoi 划分技术将图像域 $\boldsymbol{D}$ 划分为子区域 (Li 和 Li, 2010)。对给定生成点集,$\boldsymbol{G}=\{(u_j,v_j):(u_j,v_j)\in \boldsymbol{D};j=1,\cdots,m\}$,Voronoi 划分将 $\boldsymbol{D}$ 划分为 m 个子区域 (称为 Voronoi 多边形),$\boldsymbol{P}=\{\boldsymbol{P}_j:j=1,\cdots,m\}$,其中,$\boldsymbol{P}_j$ 由生成点(u_j, v_j)构造而成,即 $\boldsymbol{P}_j$ 中的任意一点(x, y)与生成点(u_j, v_j)间的距离小于距生成点集中其他生成点的距离:

$$\boldsymbol{P}_j=\{(x,y);d((x,y),(u_j,v_j))\leqslant d((x,y),(u_{j'},v_{j'})),(u_j,v_j),(u_{j'},v_{j'})\in \boldsymbol{G},j\neq j\} \quad (1)$$

式中,d 为平面上两点间的欧几里德距离。图 1 所示为由 6 个随机分布在正方形图像域上的生成点(实心点)构造而成的 Voronoi 划分图,图中,正方形内部的实线为 Voronoi 多边形的边界线,而虚线则为近邻生成点间的连线,而空心圆为像素格点。可以看出 Voronoi 多边形的边界线为相应的生成点间连线线段的垂直中分线。

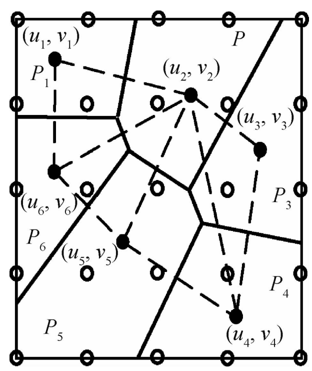

图 1 由 6 个生成点构造的 Voronoi 划分

假设生成点均匀分布于图像域 $\boldsymbol{D}$ 中,并且各生成点的分布相互独立。因此,生成点集的先验概率密度函数为:

$$p(\boldsymbol{G}\mid m)=\prod_{j=1}^{m}p(u_j,v_j)=\prod_{j=1}^{m}\frac{1}{|\boldsymbol{D}|}=|\boldsymbol{D}|^{-m} \quad (2)$$

式中,$|\boldsymbol{D}|$为图像域 $\boldsymbol{D}$ 的面积。对于 Voronoi 划分的生成点数 m,假设其满足均值为 λ 的泊松分布,因此其概率密度函数为:

$$p(m)=\frac{\lambda^m}{m!}\exp(-\lambda) \tag{3}$$

为每个 Voronoi 多边形 P_j 分配一个标号变量 $\boldsymbol{L}_j\in\{1,\cdots,k\}$，以表征其隶属的目标类，其中 k 为待分割图像的目标类总数，本文中设该数值为已知，而每个目标类的几何区域则由一组 Voronoi 多边形拟合而成。显然，对所有 Voronoi 多边形的标号集合 $\boldsymbol{L}=\{\boldsymbol{L}_j;\ j=1,\cdots,m\}$ 形成了一个随机标号场，而该随机场的每个实现对应于多视 SAR 图像 $\boldsymbol{Z}$ 的一种分割，记标号场所有可能的实现构成的空间记为 $\boldsymbol{\Omega}_L$。为了表达邻域 Voronoi 多边形标号的相关性，本文将定义在规则格点上的 MRF 模型扩展到 Voronoi 划分图上，即假设标号场 $\boldsymbol{L}$ 的概率密度函数具有如下形式：

$$p(\boldsymbol{L}\mid \boldsymbol{G},m)=\frac{1}{A}\exp\Big(-\sum_{\{\boldsymbol{L}_j,\boldsymbol{L}_{j'}\}\in \boldsymbol{NP}}\eta t(\boldsymbol{L}_j,\boldsymbol{L}_{j'})\Big) \tag{4}$$

式中，$\boldsymbol{NP}$ 为给定 Voronoi 划分图中所有邻域 Voronoi 多边形对的集合，任意两个 Voronoi 多边形互为邻域当且仅当它们具有共同的边界；A 为归一化常数，由对式(4)分子项所有可能的标号值求和得到；$\boldsymbol{\eta}$ 为邻域 Voronoi 多边形的空间作用参数，在本文方法中假设该参数为已知；$t(x,y)$ 为指示函数，

$$t(x,y)=\begin{cases}0, & 若\quad x=y\\ 1, & 若\quad x\neq y\end{cases} \tag{5}$$

由以上讨论可以看出，图像域 $\boldsymbol{D}$ 上的 Voronoi 划分 $\boldsymbol{P}$ (或生成点集 $\boldsymbol{G}$)以及定义在 $\boldsymbol{P}$ 上的标号场 $\boldsymbol{L}$ 完备地刻画了图像 $\boldsymbol{Z}$ 的分割。进一步假设，同一个 Voronoi 多边形 $\boldsymbol{P}_j$ 中具有标号 $\boldsymbol{L}_j=l$ 的随机变量 $\boldsymbol{Z}_i$ 服从同一独立的 Gamma 分布(Lee 等, 1994; Dong 等, 2003)，其概率密度函数可表示为：

$$p(\boldsymbol{Z}_i\mid (x_i,y_i)\in \boldsymbol{P}_j,\boldsymbol{L}_j=l,\boldsymbol{\beta}_l)=\frac{1}{\Gamma(\alpha)}\frac{\boldsymbol{Z}_i^{\alpha-1}}{\boldsymbol{\beta}_l^{\alpha}}\exp\Big(-\frac{\boldsymbol{Z}_i}{\boldsymbol{\beta}_l}\Big) \tag{6}$$

式中，$\Gamma(\cdot)$ 为 Gamma 函数，$\boldsymbol{\beta}_l$ 为 Gamma 分布的尺度参数，α 为 Gamma 分布的形状参数。对多视 SAR 图像，α 等于其视数(Lee 等, 1994; Dong 等, 2003)。

根据式(6), Voronoi 多边形 $\boldsymbol{P}_j$ 中所有像素强度变量的联合概率密度函数为：

$$p(\boldsymbol{Z}_j\mid \boldsymbol{L}_j=l,\boldsymbol{\beta}_l)=\prod_{(x_i,y_i)\in \boldsymbol{P}_j}\frac{1}{\Gamma(\alpha)}\frac{\boldsymbol{Z}_i^{\alpha-1}}{\boldsymbol{\beta}_l^{\alpha}}\exp\Big(-\frac{\boldsymbol{Z}_i}{\boldsymbol{\beta}_l}\Big) \tag{7}$$

式中，$\boldsymbol{Z}_j=\{\boldsymbol{Z}_i;\ (x_i,\ y_i)\in \boldsymbol{P}_j\}$。假设对所有的 Voronoi 多边形上述联合概率分布亦为相互独立，则多视 SAR 图像模型可以表达如下：

$$p(\boldsymbol{Z}\mid \boldsymbol{L},\boldsymbol{G},\boldsymbol{\beta},m)=\prod_{j=1}^{m}p(\boldsymbol{Z}_j\mid \boldsymbol{L}_j)=\prod_{j=1}^{m}\prod_{(x_i,y_i)\in \boldsymbol{P}_j}\frac{1}{\Gamma(\alpha)}\frac{\boldsymbol{Z}_i^{\alpha-1}}{\boldsymbol{\beta}_l^{\alpha}}\exp\Big(-\frac{\boldsymbol{Z}_i}{\boldsymbol{\beta}_l}\Big) \tag{8}$$

式中，$\boldsymbol{\beta}=(\boldsymbol{\beta}_1,\cdots,\boldsymbol{\beta}_k)$。

为了实现图像分割，需要得到在已知图像 $\boldsymbol{Z}$ 和参数 $\boldsymbol{\beta}$ 条件下标号场 $\boldsymbol{L}$ 的条件概率密度函数。根据贝叶斯定理，上述条件概率密度函数为：

$$\begin{aligned}p(\boldsymbol{L},\boldsymbol{G},m\mid \boldsymbol{Z},\boldsymbol{\beta})&=\frac{p(\boldsymbol{Z}\mid \boldsymbol{L},\boldsymbol{\beta})p(\boldsymbol{L}\mid \boldsymbol{G},m)p(\boldsymbol{G}\mid m)p(m)}{p(\boldsymbol{Z}\mid \boldsymbol{\beta})}=\\ &\frac{1}{p(\boldsymbol{Z}\mid \boldsymbol{\beta})}\times|\boldsymbol{D}|^{-m}\times\frac{\lambda^m}{m!}\exp(-\lambda)\times\\ &\prod_{j=1}^{m}\prod_{(x_i,y_i)\in \boldsymbol{P}_j}\frac{1}{\Gamma(\alpha)}\frac{\boldsymbol{Z}_i^{\alpha-1}}{\boldsymbol{\beta}_l^{\alpha}}\exp\Big(-\frac{\boldsymbol{Z}_i}{\boldsymbol{\beta}_l}\Big)\times\\ &\frac{1}{A}\exp\Big[-\sum_{\{\boldsymbol{L}_j,\boldsymbol{L}_{j'}\}\in \boldsymbol{NP}}\eta t(\boldsymbol{L}_j,\boldsymbol{L}_{j'})\Big]\end{aligned} \tag{9}$$

由于式中 A 和 $p(\boldsymbol{Z}|\boldsymbol{\beta})$ 与标号场 $\boldsymbol{L}$ 无关，因此，求取多视 SAR 图像分割优化解时忽略这两项。

3 EM/MPM 算法

图像模型建立完成后，采用 EM/MPM 算法进行图像分割。本文提出的 EM/MPM 多视 SAR 图像分割方法由两个基本算法组成：(1)MPM 算法用于图像分割；(2)EM 算法用于 Gamma 分布参数 $\boldsymbol{\beta}$ 的估计。

3.1 MPM 多视 SAR 图像分割算法

MPM 分割算法假定参数集 $\boldsymbol{\beta}$ 是已知的，它的基本思想在于将图像分割问题表达为优化问题，其中的优化准则为最小化误分割像素数的期望值(Comer 和 Delp, 2000)。最小化该期望值等价于对所有标号 $l\in\{1,\cdots,k\}$ 以及所有 Voronoi 多边形 $\boldsymbol{P}_j(j=1,\cdots,m)$ 使得 $p(\boldsymbol{L}_j=l,\ \boldsymbol{G}\mid \boldsymbol{Z}=z)$ 最大(Marroquin 等, 1987)。为了实现标号场 $\boldsymbol{L}$ 的 MPM 估计，需要对每一个 $\boldsymbol{P}_j$ 找到一个 l 值，使得如下边缘概率最大，

$$p(\boldsymbol{L}_j=l\mid \boldsymbol{Z}=z)=p(l,\boldsymbol{G}\mid \boldsymbol{Z},\boldsymbol{\beta})=\sum_{l\in \boldsymbol{\Omega}_{l,j},\boldsymbol{G}\in \boldsymbol{\Omega}_G}p(l,\boldsymbol{G}\mid \boldsymbol{Z},\boldsymbol{\beta}) \tag{10}$$

式中，$\Omega_{l,j}=\{\boldsymbol{l};l_j=l\}$；$\boldsymbol{\Omega}_{\boldsymbol{G}}$ 为生成点集的值空间；l 为标号场 $\boldsymbol{L}$ 的实现。实际上，精确计算式(10)的边缘概率是难以实现的。为了计算 MRF 的 MPM 估计，

Marroquin 等人(1987)提出了边缘概率近似估计算法,本文采用该算法近似估计式(10)的边缘概率。其基本过程包括(Comer 等, 2011):设计随机采样器,并依式(9)的概率密度函数生成离散时间马尔可夫链 $\boldsymbol{L}(t)=\{\boldsymbol{L}_j(t);j=1,\cdots,m\}$,而 $\boldsymbol{L}(t)$ 收敛于标号场 $\boldsymbol{L}$,即对任意给定标号场的初始实现 $l(0)$,则,

$$\lim_{t\to\infty}p(\boldsymbol{L}(t)=l,\boldsymbol{G}\mid \boldsymbol{Z}=\boldsymbol{z},\boldsymbol{L}(0)=l(0))=p(l,\boldsymbol{G}\mid \boldsymbol{z},\boldsymbol{\beta}) \tag{11}$$

由于迭代采样中任意采样时刻只能改变标号场的某一个分量 $\boldsymbol{L}_j$,由此定义:

$$a_{l,j}\equiv\begin{cases}1, & 若\quad \boldsymbol{L}_j(t)=l\\ 0, & 若\quad \boldsymbol{L}_j(t)\neq l\end{cases} \tag{12}$$

则有,

$$p(\boldsymbol{L}_j=l,\boldsymbol{G}\mid \boldsymbol{z},\boldsymbol{\beta})\approx\frac{1}{T_j}\sum_{t=1}^{T_j}a_{l,j}(t),\quad \forall l,j \tag{13}$$

式中,T_j 为随机采样器访问 $\boldsymbol{L}_j$ 的总次数。式(13)即为标号场 $\boldsymbol{L}$ 的 MPM 估计。

本文采用 M-H (Metropolis-Hastings)算法设计随机采样器。为了完备地采样$(\boldsymbol{L},\boldsymbol{G})$,设计了如下移动操作。对每次迭代采样需要遍历所有的移动操作。

(1)改变标号场。对当前标号场 $\boldsymbol{L}=\{\boldsymbol{L}_j;j=1,\cdots,m\}$ 以等概率$(1/m)$在$\{1,\cdots,m\}$抽取任意值(如 j),本次迭代改变 $\boldsymbol{L}_j$ 而其他标号保持不变。候选标号 $\boldsymbol{L}_j^*$ 以等概率$(1/k)$在$\{1,\cdots,k\}$抽取,并满足条件:$\boldsymbol{L}_j^*\neq\boldsymbol{L}_j$。改变 $\boldsymbol{L}_j$ 的接受概率可计算为:

$$a_L(\boldsymbol{L}_j,\boldsymbol{L}_j^*)=\min\left\{1,\ \frac{\prod_{(x_i,y_i)\in\boldsymbol{P}_j}\frac{1}{(\boldsymbol{\beta}_{\boldsymbol{L}_j^*})^{\alpha}}\exp\left[-\frac{\boldsymbol{Z}_i}{\boldsymbol{\beta}_{\boldsymbol{L}_j^*}}\right]\exp\left[-\sum_{P_{j'}\in \boldsymbol{NP}_j}\eta t(\boldsymbol{L}_j^*,\boldsymbol{L}_{j'})\right]}{\prod_{(x_i,y_i)\in\boldsymbol{P}_j}\frac{1}{(\boldsymbol{\beta}_{\boldsymbol{L}_j})^{\alpha}}\exp\left[-\frac{\boldsymbol{Z}_i}{\boldsymbol{\beta}_{\boldsymbol{L}_j}}\right]\exp\left[-\sum_{P_{j'}\in \boldsymbol{NP}_j}\eta t(\boldsymbol{L}_j,\boldsymbol{L}_{j'})\right]}\right\} \tag{14}$$

式中,$\boldsymbol{NP}_j$ 为 $\boldsymbol{P}_j$ 的邻域 Voronoi 多边形集合。

(2)位移生成点。对当前生成点集合 $\boldsymbol{G}=\{(u_j,v_j)\in\boldsymbol{D};j=1,\cdots,m\}$,以等概率$(1/m)$在$\{1,\cdots,m\}$抽取任意值(如 j),本次迭代改变(u_j,v_j)而其他生成点保持不变。候选生成点(u_j^*,v_j^*)在当前多边形 $\boldsymbol{P}_j$ 中均匀抽取。位移某一生成点仅改变与该生成点相应的多边形及其邻域多边形。改变(u_j,v_j)的接受概率为:

$$a_{(u,v)}((u_j,v_j),(u_j^*,v_j^*))=\min\left\{1,\ \frac{\prod_{\boldsymbol{P}_{j'}\in\{\boldsymbol{P}_j^*,\boldsymbol{PN}_j^*\}}\prod_{(x_i,y_i)\in\boldsymbol{P}_{j'}}\frac{1}{(\boldsymbol{\beta}_{\boldsymbol{L}_{j'}})^{\alpha}}\exp\left[-\frac{\boldsymbol{Z}_i}{\boldsymbol{\beta}_{\boldsymbol{L}_{j'}}}\right]}{\prod_{\boldsymbol{P}_{j'}\in\{\boldsymbol{P}_j,\boldsymbol{PN}_j\}}\prod_{(x_i,y_i)\in\boldsymbol{P}_{j'}}\frac{1}{(\boldsymbol{\beta}_{\boldsymbol{L}_{j'}})^{\alpha}}\exp\left[-\frac{\boldsymbol{Z}_i}{\boldsymbol{\beta}_{\boldsymbol{L}_{j'}}}\right]}\right\} \tag{15}$$

(3)增加或删除生成点。设当前生成点集合为 $\boldsymbol{G}=\{(u_1,v_1),\cdots,(u_j,v_j),\cdots(u_m,v_m)\}$。对于增加生成点操作,首先在图像域 $\boldsymbol{D}$ 中均匀抽取候选生成点并标记为 $m+1$,即(u_{m+1}^*,v_{m+1}^*)。候选生成点集合可表示为 $\boldsymbol{G}^*=\{(u_1,v_1),\cdots,(u_j,v_j),\cdots(u_m,v_m),(u_{m+1}^*,v_{m+1}^*)\}$。依据式(1),$\boldsymbol{G}^*$ 构造候选 Voronoi 划分 $\boldsymbol{P}^*=\{\boldsymbol{P}_1^*,\cdots,\boldsymbol{P}_m^*,\boldsymbol{P}_{m+1}^*\}$。如果$(u_{m+1}^*,v_{m+1}^*)$位于 $\boldsymbol{P}_j$ 中,则(u_{m+1}^*,v_{m+1}^*)生成新多边形 $\boldsymbol{P}_{m+1}^*$ 并仅仅改变 $\boldsymbol{P}_j$ 及其邻域多边形。以等概率$(1/k)$在$\{1,\cdots,k\}$抽取随机数作为多边形 $\boldsymbol{P}_{m+1}^*$ 的标号 $\boldsymbol{L}_{m+1}^*$。由此,候选标号场为 $\boldsymbol{L}^*=\{\boldsymbol{L}_1^*,\cdots,\boldsymbol{L}_j^*,\cdots,\boldsymbol{L}_m^*,\boldsymbol{L}_{m+1}^*\}$,其中对应于$\{\boldsymbol{P}_1^*,\cdots,\boldsymbol{P}_m^*\}$的标号$\{\boldsymbol{L}_1^*,\cdots,\boldsymbol{L}_m^*\}$保持当前标号不变。增加生成点操作以如下概率被接受:

$$a_{G+}(\boldsymbol{G},\boldsymbol{G}^*)=\min\{1,R\} \tag{16}$$

式中,

$$R=\frac{\prod_{j=1}^{m+1}\prod_{(x_i,y_i)\in\boldsymbol{P}_j^*}\frac{1}{(\boldsymbol{\beta}_{\boldsymbol{L}_j^*})^{\alpha}}\exp[-\boldsymbol{Z}_i/\boldsymbol{\beta}_{\boldsymbol{L}_j^*}]}{\prod_{j=1}^{m}\prod_{(x_i,y_i)\in\boldsymbol{P}_j}\frac{1}{(\boldsymbol{\beta}_{\boldsymbol{L}_j})^{\alpha}}\exp[-\boldsymbol{Z}_i/\boldsymbol{\beta}_{\boldsymbol{L}_j}]}\times\frac{\prod_{j=1}^{m+1}\exp\left(\sum_{P_{j'}^*\in PN_j^*}\eta t(\boldsymbol{L}_j^*,\boldsymbol{L}_{j'}^*)\right)\Big/\sum_{l=1}^{k}\exp\left(\sum_{P_{j'}^*\in PN_j^*}\eta t(l,\boldsymbol{L}_{j'}^*)\right)}{\prod_{j=1}^{m}\exp\left(\sum_{P_{j'}^*\in PN_j^*}\eta t(\boldsymbol{L}_j,\boldsymbol{L}_{j'})\right)\Big/\sum_{l=1}^{k}\exp\left(\sum_{P_{j'}\in PN_j}\eta t(l,\boldsymbol{L}_{j'})\right)} \tag{17}$$

删除生成点操作是增加生成点操作的对偶操作,因此其接收概率为:

$$a_{G-}(\boldsymbol{G},\boldsymbol{G}^*)=\min\{1,1/R\} \tag{18}$$

3.2 EM 参数估计算法

为了实现上述 M-H 采样,必须对参数 $\boldsymbol{\beta}$ 进行估计。本文采用 EM 算法 (Masuda 等, 2011; 夏怀英和郭平, 2011; 徐振华 等, 2011) 估计该参数。EM 算法通过迭代过程近似得到最大或然率 ML(Maximum-likelihood)估计值。每次迭代分两步完成 ML 估计:计算期望值和最大化期望值。如果设 $\boldsymbol{\beta}(\tau)$ 为在第 τ 次迭代时的参数 $\boldsymbol{\beta}$ 估计值,则该次迭代中 $\boldsymbol{\beta}$ 的期望值计算如下,

$$Q(\boldsymbol{\beta},\boldsymbol{\beta}(\tau-1))=$$

$$E[\log p(\boldsymbol{Z}\mid \boldsymbol{L},\boldsymbol{\beta})\mid \boldsymbol{Z}=z,\boldsymbol{\beta}(\tau-1)]+$$
$$E[\log p(\boldsymbol{L}\mid \boldsymbol{\beta})\mid \boldsymbol{Z}=z,\boldsymbol{\beta}(\tau-1)] \qquad (19)$$

由于标号场 $\boldsymbol{L}$ 的概率密度函数与 $\boldsymbol{\beta}$ 无关，由此忽略式(19)等式右边的第二项。$\boldsymbol{\beta}(\tau)$ 则是通过最大化 $Q(\boldsymbol{\beta},\boldsymbol{\beta}(\tau-1))$ 得到的，即 $\boldsymbol{\beta}(\tau)$ 满足，

$$Q(\boldsymbol{\beta}(\tau),\boldsymbol{\beta}(\tau-1))\geqslant Q(\boldsymbol{\beta},\boldsymbol{\beta}(\tau-1)) \quad \forall \boldsymbol{\beta}\in \boldsymbol{\Omega}_{\beta} \qquad (20)$$

式中，$\boldsymbol{\Omega}_{\beta}$ 为 $\boldsymbol{\beta}$ 的取值空间。将式(8)代入式(19)，对其求导并设该导数为零，则可解 $\boldsymbol{\beta}(\tau)=(\boldsymbol{\beta}_1(\tau),\cdots,\boldsymbol{\beta}_k(\tau))$ 得，

$$\boldsymbol{\beta}_l(\tau)=\frac{1}{\alpha N_l(\tau)}\sum_{\boldsymbol{P}_j\in \boldsymbol{P}_l} p(\boldsymbol{L}_j=l\mid \boldsymbol{Z},\boldsymbol{\beta}(\tau-1))\sum_{(x_i,y_i)\in \boldsymbol{P}_j} \boldsymbol{Z}_i \qquad (21)$$

式中，$\boldsymbol{P}_l=\{\boldsymbol{P}_j;\ \boldsymbol{L}_j=l\}$，$N_l(\tau)=\sum_{\boldsymbol{P}_j\in \boldsymbol{P}_l} N_j p(\boldsymbol{L}_j=l\mid \boldsymbol{Z},\boldsymbol{\beta}(\tau-1))$，$N_j=\#\boldsymbol{Z}_j$。从计算角度看，得到概率密度 $p(\boldsymbol{L}_j=l\mid \boldsymbol{Z},\boldsymbol{\beta})$ 的实际值是不可能的。因此本文用式(13)得到 $p(\boldsymbol{L}_j=l\mid \boldsymbol{Z},\boldsymbol{\beta})$ 的估计值，以期计算式(21)，从而获得参数 $\boldsymbol{\beta}$ 的估计值。

3.3　EM/MPM 算法流程

EM/MPM 算法综合运用了上述 EM 和 MPM 算法。其中 MPM 算法用于图像分割，EM 算法用于参数估计。EM/MPM 算法的实现步骤如下：

(1)初始化参数 $\boldsymbol{\beta}$，记为 $\boldsymbol{\beta}(0)$。

(2)采用参数 $\boldsymbol{\beta}(\tau-1)$，执行 T_p 次的 MPM 算法(本文实验中采用 500 次)，利用式(13)得到标号场 $\boldsymbol{L}$ 的 MPM 估计。

(3)利用步骤(2)中得到的标号场 $\boldsymbol{L}$ 的 MPM 估计，分别代入式(21)得到参数 $\boldsymbol{\beta}$ 的估计值 $\boldsymbol{\beta}(\tau)$。

(4)返回步骤(2)，直到达到预订的总循环次数或者参数 $\boldsymbol{\beta}$ 收敛到稳定值。

4　实验结果及讨论

为了验证本文算法的可行性和有效性，分别对模拟 SAR 图像及真实 SAR 图像进行了分割实验。

首先，生成视数为 4 同质区域为 5 个、尺度为 128×128 像素的模拟 SAR 图像。图 2(a)为生成的模拟图像的同质区域模板，其中编号 1—5 分别代表不同的同质区域。表 1 列出各同质区域的 Gamma 分布参数。

在构建模拟 SAR 图像时，不同同质区域对应的 Gamma 分布尺度参数选择了较为接近的数值。图 2(b)所示为生成的模拟图像。

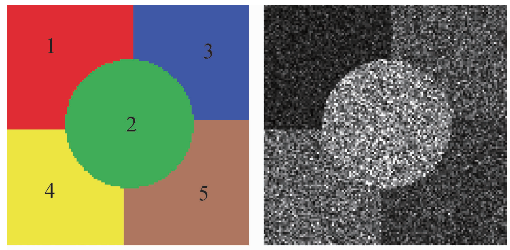

(a) 几何模板　(b) 模拟SAR图像

图 2　模拟图像的生成

表 1　模拟图像各同质区域的 Gamma 分布参数

参数	同质区域				
	1	2	3	4	5
α	4	4	4	4	4
β	10	35	20	25	15

由于本文方法可以看作是基于像素的 MRF 模型的扩展，因此采用本文方法和基于像素的 MRF 分割方法(Cao 等，2005; Comer 和 Delp，2000)分别对图 2(b)中的模拟 SAR 图像进行了分割实验，分割结果见图 3。在本文分割方法中设置 EM 参数估计的迭代次数为 100，获取 MPM 分割优化解的迭代次数为 500。图 3(a)和图 3(b)分别为本文方法中初始 Voronoi 多边形个数为 64 对应的最终 Voronoi 划分结果(每一个 Voronoi 多边形被随机分配一种彩色进行显示，最终的 Voronoi 多边形数为 30)和最优分割结果，图 3(c)为基于像素的 MRF 算法分割结果，其中图 3(b)和图 3(c)中各同质区域分别以算法估计得到的该区域像素灰度平均值进行显示。对比两种分割结果可以发现，本文算法将模拟 SAR 图像中 5 个同质区域较好地分割开来，同时较好地拟合了各同质区域的边界，但基于像素 MRF 方法的分割结果虽然在各个同质区域像素灰度平均值上和本文算法相接近，但是却将不同的区域混淆在一起，原因在于基于像素的 MRF 模型只考虑了邻域像素之间的相关性，没有考虑区域内像素间及区域与区域之间的相互关系，因而不能克服 SAR 图像斑点噪声带来的图像分割困难。

(a) Voronoi划分　(b) 最优分割　(c) MRF分割结果

图 3　分割结果

表 2 列出两种算法估计得到的 Gamma 分布的尺度参数的估计值及与估计误差值。与表 1 列出的实际 Gamma 分布参数比较,可以看出,本文方法不仅可以精确分割图像,还可以得到更为准确的分布参数估计值。

表 2 各同质区域尺度分布参数估计值及其误差

	参数	同质区域				
		1	2	3	4	5
本文方法	$\boldsymbol{\beta}_e$	10.05	33.64	20.04	24.62	15.12
	$e_\beta/\%$	0.47	1.37	0.04	0.38	0.12
MRF 方法	$\boldsymbol{\beta}_e$	11.27	35.37	16.18	24.38	12.50
	$e_\beta/\%$	1.27	0.37	3.72	0.62	2.50

为了从视觉角度评估本文最优分割结果,本文提取了分割区域的轮廓线,如图 4(a),并将该轮廓线分别叠加在最终的 Voronoi 划分图上和模拟 SAR 图像上,分别见图 4(b)和图 4(c)。从图 4(b)可以看出同质区域可以由一定数量的 Voronoi 多边形拟合而成,尤其是最不容易拟合的圆形在本算法中亦能够很好的拟合。而图 4(c)则显示分割同质区域轮廓线和原始图像叠加效果,说明算法可以得到很高的分割精度。尽管构造模拟图像时各个区域之间的 Gamma 分布参数相差不大,但算法仍然能够准确地区分它们,说明本文算法具有很强的区分不同同质区域的能力。

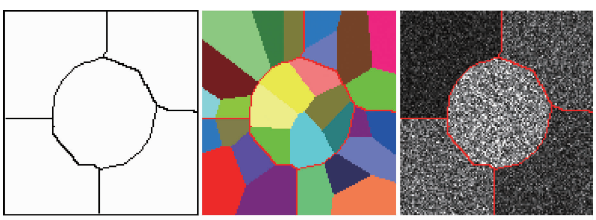

(a) 同质区域轮廓　(b) 轮廓线和Voronoi划分的叠加　(c) 轮廓线和模拟图像的叠加

图 4 模拟图像分割结果的视觉评价

图 5 所示为本文方法得到的该模拟 SAR 图像同质区域内像素强度 Gamma 分布尺度参数 $\boldsymbol{\beta}$ 的变化,其中 C1—C5 表示与生成模拟图像时采用的模板相对应的类别。可以看出各同质区域的 Gamma 分布的尺度参数很快收敛到各自的稳态值。

为了对提出的算法进行定量的评估,将生成模拟 SAR 图像的模板作为参考图像,与本文算法和基于像素的 MRF 算法得到的分割结果(图 3(b)和图 3(c))逐一像素进行正确性分类对比,计算得到混淆矩阵,并据此分别计算出产品精度、用户精度和总精度(表 3)。

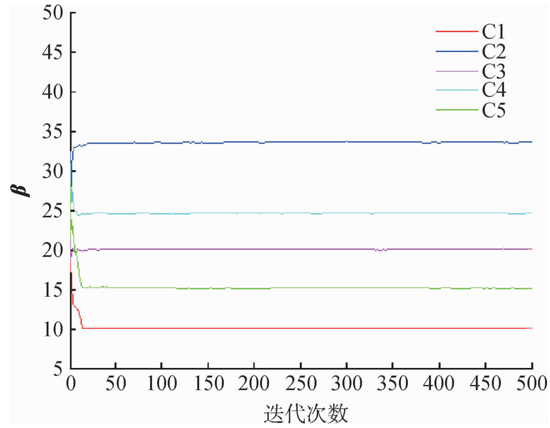

图 5 $\boldsymbol{\beta}$ 参数变化

表 3 用户精度、产品精度、总精度和 Kappa 值 /%

	精度	同质区域				
		1	2	3	4	5
本文方法	用户精度	99.61	99.06	99.63	99.12	99.22
	产品精度	99.94	99.20	99.42	99.84	98.41
	总精度			99.34		
	Kappa			0. 99		
MRF 方法	用户精度	51.01	75.93	65.37	51.48	36.86
	产品精度	26.42	79.98	65.35	56.15	40.26
	总精度			44.59		
	Kappa			0.31		

本文中,用户精度表示对分类结果中所有像素,其所具有的类型与参考图像类型相同的概率;产品精度表示相对于参考图像中的任意一个像素,分类图上同一像素的分类结果与其相一致的条件概率;总精度表述的是每一个像素,所分类的结果与参考图像的实际类型相一致的概率。对于本文方法,各项精度指标均达 98% 以上。根据上述精度可以计算该分割算法的 Kappa 值,即通过把所有参考图像中的像元总数乘以混淆矩阵对角线的和,再减去某一类参考图像像元总数与被误分成该类像元总数之积对所有类别求和的结果,再除以总像元数的平方差减去某一类中参考图像像元总数与该类中被分类像元总数之积对所有类别求和的结果所得到的。Kappa 值越大,分类结果的精度越高。本算法中计算得到 Kappa=0.99。对一般分类器该值达 0.8 以上即为优质分类器 (Congaltonr 和 Green, 2008)。对于基于像素的 MRF 分割方法总体精度仅为 44.59%,Kappa 值仅为 0.31,对比可以发现本文算法的有效性和准确性。

在基于 MPM 算法分割过程中,划分的多边形个数 m 为变量,在分割之前需要对 m 进行初始值设

置。为了验证初始多边形对划分后用于拟合同质区域的多边形数量或 Voronoi 多边形包含的平均像素数的影响,本文进行了不同初始多边形个数(m 分别设置为 48、64、80、96 和 112)的对比分割实验。图 6 所示为 500 次迭代对应不同初始 Voronoi 多边形的分割过程中 m 的变化曲线图,其中横轴表示迭代次数,纵轴表示 m 值。从图 6 可以发现对于不同的初始值 m,在迭代循环过程中,多边形的数目 m 很快由初始值收敛至某一稳定值附近,且最终划分的 Voronoi 多边形数均趋近于稳定值。如对上述初始设置的 m 值,经算法 500 次迭代最终 Voronoi 数分别为 29、30、36、35 和 33。实验结果表明,本文算法总是试图用最少数量的 Voronoi 多边形拟合同质区域。该实验说明初始多边形的个数设置对最终划分多边形的个数影响很小。因此,虽然本文中划分方法属于随机方法,但是该算法对用于拟合各个同质区域的多边形的数量具有较好的稳定性。此外,采用本文方法,对图 7 中视数分别为 2、3、4,同质区域(类别)个数分别为 4、3、4 的 3 幅真实 RADARSAT-Ⅰ/Ⅱ SAR 强度图像进行了分割实验。图 8(a)—(c)为最优的分割结果,图 8(d)—(f)为提取的分割同质区域边界线,图 8(g)—(i)和图 8(j)—(l)分别为边界线和最终 Voronoi 划分及原始图像叠加的结果。从图 8 结果可以看出,采用本文方法对不同视数的真实 SAR 图像分割均取得了较好的效果。

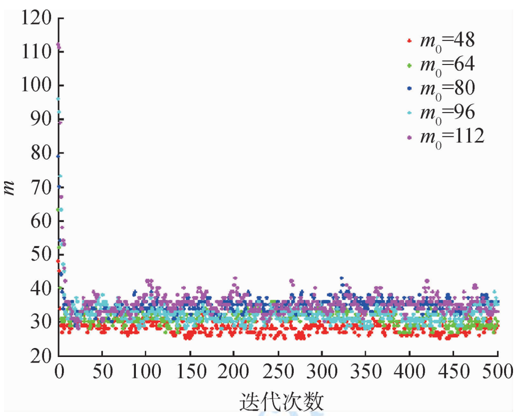

图 6　500 次迭代 m 变化曲线

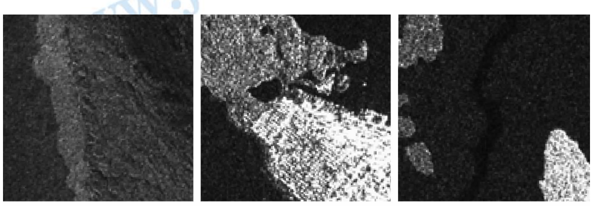

(a)　(b)　(c)

图 7　待分割图像

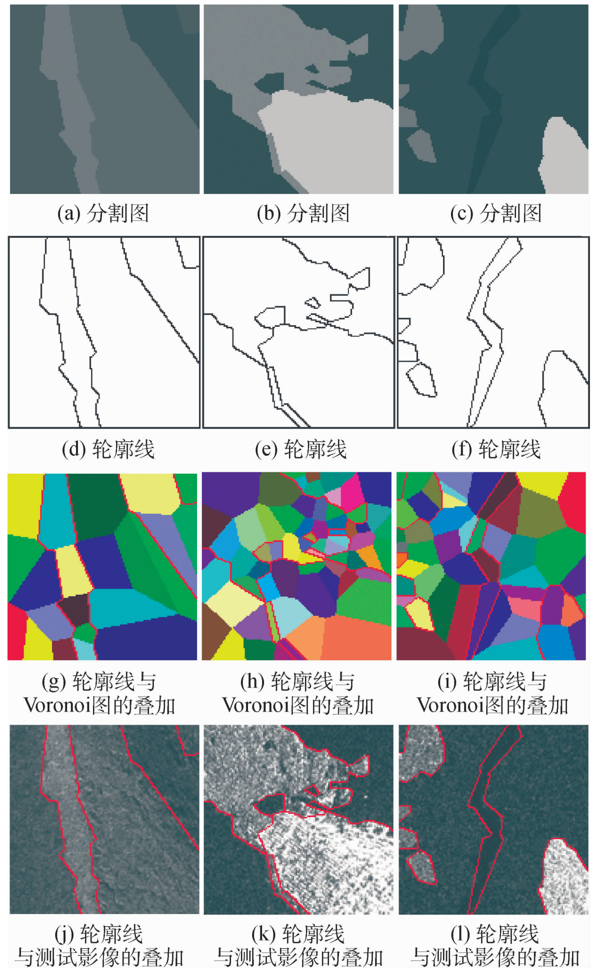

图 8　真实 SAR 图像分割结果视觉评价

5　结　论

针对基于区域和统计的分割方法进行研究,提出了一种结合 Voronoi 划分技术、EM/MPM 算法的多视 SAR 图像分割方法,分别对模拟 SAR 图像和真实 SAR 图像进行了分割实验,并和传统的基于像素的 MRF 分割方法进行了对比,定性和定量的测试结果验证了本文方法的有效性、可靠性和准确性。在实验过程中,进行了初始划分多边形的个数设置对最终划分多边形数量的影响分析,发现初始多边形的个数对最终的划分多边形的个数几乎没有影响,这也证明了本文算法对于划分的稳定性。虽然本文实验结果验证了利用 Voronoi 多边形拟合同质区域几何形状的可行性,但由于仅仅设计了移动生成点以及增加和删除生成点两种简单的操作改变 Voronoi 多边形的形态,因此在某些情况下对同质区域边界(如非光滑边缘)的拟合结果不甚理想。在今后的工作中,对如何进一步提高同质区域

边缘的拟合精度需要继续从理论上进行研究,如设计其他可以改变 Voronoi 多边形形态的操作,各种不同的划分技术(规则、Voronoi、Poisson 和 Leave 划分)对边界拟合的作用和影响;在优化算法上的改进可以部分解决同质区域边界拟合精度,在未来的工作将进一步借鉴和比较不同优化算法的适用性;本文方法假定多视 SAR 图像像素强度服从 Gamma 分布的形状参数等于其视数,这一条件只有在各视之间相互独立的情况下得以满足,但实际上各视之间不可避免的存在着相关性,因此,接下来应进一步将形状参数 α 作为参数进行估计来完成 SAR 图像分割。

参考文献(References)

Cao Y, Sun H and Xu X. 2005. An unsupervised segmentation method based on MPM for SAR images. IEEE Geoscience and Remote Sensing Letters, 2(1): 55−58 [DOI: 10.1109/LGRS.2004.839649]

Comer M L and Delp E J. 2000. The EM/MPM algorithm for segmentation of textured images: analysis and future experimental results. IEEE Transactions on Image Processing, 9(10): 1731−1744 [DOI: 10.1109/83.869185]

Comer M L, Bouman C A, De Graef M and Dimmons J P. 2011. Bayesian methods for image segmentation. JOM Journal of the Minerals, Metals and Materials Society, 63(7): 55−57 [DOI: 10.1007/s11837-011-0113-3]

Congaltonr G and Green K. 2008. Assessing the Accuracy of Remotely Sensed Data: Principles and Practices. Boca Raton: CRC Press, 169−190

Dong Y, Forster B C and Milne A K. 2003. Comparison of radar image segmentation by Gaussian-and Gamma-Markov random field models. International Journal of Remote Sensing, 24(4): 711−722 [DOI: 10.1080/01431160210000013322]

Dryden I L, Farnoosh R and Taylor C C. 2006. Image segmentation using Voronoi polygons and MCMC, with application to muscle fibre images. Journal of Applied Statistics, 33(6): 609−622 [DOI: 10.1080/02664760600679825]

Green P. 1995. Reversible jump MCMC computation and Bayesian model determination. Biometrika, 82(4): 711−732 [DOI: 10.1093/biomet/82.4.711]

Lee J S, Hoppel K W, Mango S A and Miller A R. 1994. Intensity and phase statistics of multilook polarimetric and interferometric SAR imagery. IEEE Transactions on Geoscience and Remote Sensing, 32(5): 1017−1028 [DOI: 10.1109/36.312890]

郦苏丹, 张翠, 王正志. 2003. 基于相似性准则的 SAR 图像分割方法. 遥感学报, 7(2): 118−124

Li Y and Li J. 2010. Segmentation of SAR intensity imagery with a Voronoi tessellation, Bayesian inference, and reversible jump MCMC algorithm. IEEE Transactions on Geoscience and Remote Sensing, 48(4): 1872−1881 [DOI: 10.1109/TGRS.2009.2033588]

Marroquin J, Mitter S and Pojjio T. 1987. Probabilistic solution of ill-posed problems in computational vision. Journal of the American Statistical Association, 82(397): 76−89

Masuda Y, Tateyama T, Wei X, Zhou J Y, Wakamiya M, Kanasaki S, Furukawa A and Chen Y W. 2011. Liver tumor detection in CT images by adaptive contrast enhancement and the EM/MPM algorithm // Proceedings of the 18th IEEE International Conference on Image Processing. Brussels, Belgium: IEEE: 1421−1424 [DOI: 10.1109/ICIP.2011.6115708]

宋晓峰, 王爽, 刘芳. 2010. 基于区域 MRF 和贝叶斯置信传播的 SAR 图像分割. 电子学报, 38(12): 2810−2815

王晓亮, 李春升. 2010. 无需先验信息的水平集 SAR 图像分割方法. 北京航空航天大学学报, 36(7): 841−844

Wong A, Yu P, Zhang W and Clausi D A. 2010. IceSynth II: synthesis of SAR sea-ice imagery using region based posterior sampling. IEEE Geoscience and Remote Sensing Letters, 7(2): 348−351 [DOI: 10.1109/LGRS.2009.2035136]

夏怀英, 郭平. 2011. 基于统计混合模型的遥感影像阴影检测. 遥感学报, 15(4): 785−791

许新征, 丁世飞, 史忠植, 贾伟宽. 2010. 图像分割的新理论和新方法. 电子学报, 38(S1): 76−82

徐振华, 黄建国, 张群飞. 2011. 基于 EM 算法的极大似然分布式量化估计融合新方法. 电子与信息学报, 33(4): 977−981

张林, 朱兆达. 2010. 基于全局 Maxflow 邻域生长算法的 SAR 图像目标分割. 南京航空航天大学学报, 42(6): 764−768

遥感学报　启功先生创刊题名

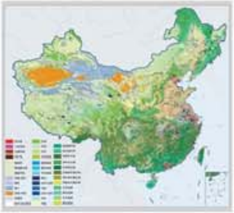

封面说明
About the Cover

2010年中国土地覆被遥感监测数据集（ChinaCover2010）

The China National Land Cover Data for 2010 (ChinaCover2010)

2010 年中国土地覆被遥感监测数据集（ChinaCover2010）由中国科学院遥感与数字地球研究所联合其他 9 个单位历时两年完成，应用 30 m 空间分辨率的环境星（HJ-1A/1B）数据，利用联合国粮农组织（FAO）的 LCCS 分类工具，构建了适用于中国生态特征的 38 类土地覆被分类系统，采用基于超算平台的数据预处理、面向对象的自动分类、地面调查获得的 10 万个野外样本以及雷达数据辅助分类相结合的方法，数据精度达到 85%。ChinaCover2010 主要基于国产卫星影像，将遥感与生态紧密结合，充足的野外样点以及严格的产品质量控制在最大程度上保证了数据的精度，可为中国生态环境变化评估以及生态系统碳估算提供基础数据支撑。（网址：http://www.chinacover.org.cn）

The China National Land Cover Data for 2010 (ChinaCover2010) has been completed after two years of team effort by the Institute of Remote Sensing and Digital Earth (RADI), Chinese Academy of Sciences (CAS), together with nine other institutions' participation. The HJ-1A/1B satellite at 30 m resolution is main data source. Based on the landscape features in China, 38 land cover classes have been defined using UN FAO Land Cover Classification System (LCCS). Super computers were used in the data preprocessing. An object-oriented method and a thorough field survey (about 100000 field samples) were used in the land cover classification, with radar imagery as auxiliary data. The overall accuracy of ChinaCover2010 is around 85%. Mainly based on domestic imagery, the products take advantage of various in situ data and strict quality control. ChinaCover2010 is a good dataset for ecological environment change assessment and terrestrial carbon budget studies. (Website: http://www.chinacover.org.cn)

遥感学报　JOURNAL OF REMOTE SENSING

YAOGAN XUEBAO（双月刊　1997年创刊）　(Bimonthly, Started in 1997)

第17卷　第4期　2013年7月25日　Vol.17 No.4 July 25, 2013

主　管	中国科学院	Superintended by	Chinese Academy of Sciences
主　办	中国科学院遥感与数字地球研究所 中国地理学会环境遥感分会	Sponsored by	Institute of Remote Sensing and Digital Earth,CAS The Associate on Environment Remote Sensing of China
主　编	顾行发	Editor-in-Chief	GU Xing-fa
编　辑	《遥感学报》编委会 北京市安外大屯路中国科学院遥感与数字地球研究所 邮编：100101　电话：86-10-64806643 http://www.jors.cn E-mail:jrs@irsa.ac.cn	Edited by	Editorial Board of Journal of Remote Sensing Add: P.O.Box 9718, Beijing 100101, China Tel: 86-10-64806643 http://www.jors.cn E-mail: jrs@irsa.ac.cn
出　版	科学出版社	Published by	Science Press
印刷装订	北京科信印刷有限公司	Printed by	Beijing Kexin Printing Co. Ltd.
总发行	科学出版社 北京东黄城根北街16号 邮政编码：100717 电话：86-10-64017032 E-mail:sales_journal@mail.sciencep.com	Distributed by	Science Press Add: 16 Donghuangchenggen North Street, Beijing 100717, China Tel: 86-10-64017032 E-mail: sales_journal@mail.sciencep.com
国外发行	中国国际图书贸易总公司 北京 399 信箱　邮政编码：100044	Overseas distributed by	China International Book Trading Corporation Add: P.O.Box 399, Beijing 100044, China

中国标准连续出版物号：ISSN 1007-4619 / CN 11-3841/TP　国内邮发代号：82-324　定价：70. 00元

CODEN YXAUAB　国外发行代号：BM 1002

ISSN 1007-4619

国内外公开发行